ELSEVIER

Sensors and Actuators A 64 (1998) 157–164

SENSORS AND ACTUATORS A PHYSICAL

High-sensitivity silicon capacitive sensors for measuring medium-vacuum gas pressures

David C. Catling *

Mail Stop 245-3, Space Science Division, NASA Ames Research Center, Moffett Field, CA 94035-1000, USA

Received 3 February 1997; revised 27 May 1997; accepted 28 May 1997

Abstract

The design, construction, and preliminary testing of an experimental capacitive silicon pressure sensor are described. The prototype sensor is designed as a robust, precision barometer suitable for measurements on the planet Mars where the mean atmospheric pressure is ~6 mbar (600 Pa). Most commercially available silicon pressure sensors tend to operate over pressure ranges ≥1 bar, or measure gauge pressure, but this sensor is specifically constructed to measure absolute pressure of 0–10 mbar with a very high sensitivity ~1 pF $mbar^{-1}$. The transductional mechanism is the deflection of a silicon diaphragm under applied pressure across a sealed vacuum cavity. Under storage conditions of 1 bar, the diaphragm displacement is mechanically constrained by an underlying stopping surface. Finite-element analysis shows that typical structures are extremely resistant to overpressure: fracture occurs at many tens of bar. The device is fabricated using a silicon fusion-bonded vacuum cavity which provides for relative insensitivity to temperature changes. © 1998 Elsevier Science S.A.

Keywords: Pressure sensors; Capacitive; Vacuum measurement

1. Introduction

This paper presents a preliminary investigation into the feasibility of using fusion-bonded capacitive micro pressure sensors for precise vacuum measurement. The effort was motivated by a planetary exploration objective to measure the global meteorology on Mars, where the average atmospheric pressure at the surface is ~600 Pa (compared to the Earth's ~10^5 Pa). On Mars, a global network of about 20 pressure sensors on the planet's surface combined with orbiter measurements can provide the data necessary to solve the fluid equations which describe the atmospheric circulation (i.e., the three-dimensional wind field around the planet and its variation in time). Surface anemometers would be unsuitable because these would only measure very local winds, strongly affected by factors such as nearby surface topography, whereas pressure gradients indicate large-scale winds. Haberle and Catling [1] have discussed the rationale and required performance of pressure sensors on Mars. The specifications are demanding: an absolute pressure range of 0–12 mbar, a resolution of 0.01 mbar, an accuracy of ±0.03 mbar, and a long-term zero drift of <0.1 mbar per year (where 1 mbar ≡ 100 Pa is the unit conventionally used in meteorology). Because pressure sensors can be miniaturized and do not require specific orientation, the resulting probes (comprising landing systems, telemetry, electrical subsystems, and housing) are small enough that 15–25 of them could be sent to Mars with just one, low-cost launch vehicle [2]. Battery power would allow operation over a Martian year (1.9 Earth years) for the detection of seasonal weather changes, or a small radioisotope power source could facilitate climate studies over many years. In either case, thermal control of −40 to +60°C inside the space probes (where pressure sensors would be housed, connected to the external atmosphere via tubing) would be necessary to ensure subsystem longevity.

Vacuum pressures from 10^{-3} to 1000 mbar are traditionally measured using either a Pirani gauge or detection of the deflection of a metallic diaphragm according to reluctance, capacitance or strain. Conventional instruments do not combine the size and performance requirements for small Mars probes. However, micromachined sensors [3–5] offer the possibility of satisfying the various demands and also have the advantage of batch fabrication. A miniature, accurate, high-resolution sensor operating over 0–10 mbar may also be useful for other applications, e.g., measurements in the Earth's upper atmosphere, and research vacuum applications where conventional gauges are currently used but smaller sensors would be more appropriate.

* Tel.: +1 415 604 1504. Fax: +1 415 604 6779. E-mail: catling@humbabe.arc.nasa.gov

PII S0924-4247(97)01616-6

Of the three main types of micro pressure sensor, piezoresistive, capacitive and resonant, the latter two hold most promise for a high-accuracy vacuum sensor. This paper deals with a preliminary investigation into using a capacitive sensor; other sensor types are also under current investigation. Most commercial micro pressure sensors use the piezoresistive technique, but capacitive sensors are intrinsically superior with lower temperature sensitivity, noise, zero drift, and power consumption [6–10]. The fractional change in capacitance for a particular pressure step is also one or two magnitudes greater than the fractional resistance change in a piezoresistive device of comparable size [11]. For accurately measuring low absolute pressure, a capacitive sensor is therefore inherently more suitable than a piezoresistive one. Despite the advantages, the use of capacitive micro pressure sensors has been very limited because of the desire for linear response in mass-produced devices (e.g., for automobiles). Silicon capacitive pressure sensors have a nonlinear output. However, the approach for research sensors is very different from the mass market because each sensor can be individually characterized and calibrated. Consequently, relatively high ($\sim$10–20%) nonlinearity can be tolerated because it can easily be overcome by remote digital processing. Repeatability is the important characteristic. Fortunately, single-crystal silicon diaphragms have negligible creep and excellent repeatability (even after pressure cycling 10^7 times [12]). Nevertheless, measuring low absolute pressures with high precision still presents design difficulties: a thin, large-area diaphragm must be used for high sensitivity but this has much deflection under normal storage conditions of 1 bar. One simple way to overcome this problem is to use a diaphragm stop, i.e., the diaphragm contacts an underlying surface at a pressure less than 1 bar but greater than the desired range. This leads to a sensor with high sensitivity at low pressure that is also subject to much lower stresses than otherwise in the normal handling environment of 1 bar.

A vacuum cavity between capacitance plates is required to make an absolute pressure sensor and eliminate zero drift from thermal expansion of trapped gas. Most research with capacitive sensors has focused on sensors comprising silicon bonded to a metallized glass substrate (see Ref. [8] and references therein). These sensors can have a large thermal coefficient of offset caused by the different thermal expansion coefficients of silicon and glass. Also inbuilt stress produced when the structure cools after bonding may subsequently cause zero drift by gradual stress relaxation. Other problems with glass are outgassing into the sealed vacuum cavity either during bonding [13,14] or afterwards. An alternative is to make vacuum cavities by silicon fusion bonding (SFB) [15–17] effected under vacuum. SFB will reduce the thermal dependence of offset of the sensor die by making an almost all-silicon structure. It can also provide an excellent sealed vacuum. Since SFB offers these potential benefits, it was adopted for the sensor investigation in this paper.

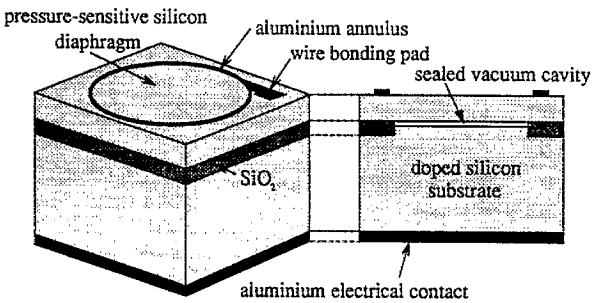

Fig. 1. A schematic picture of the capacitive pressure sensor chip. (Not to scale.)

2. Transducer description

The simple, experimental prototype (shown schematically in Fig. 1) uses a silicon diaphragm and a silicon substrate as two plates of a pressure-sensitive capacitor. The sensing part of the device is a thin, circular silicon diaphragm. This is joined to a silicon substrate by a fusion bond which forms an hermetically sealed vacuum cavity. A semi-recessed oxide (SEMIROX) layer (i.e., an oxide layer half-sunk into the silicon) supports the diaphragm and has a thickness which exceeds the cavity depth. This approximately halves the parallel capacitance at the edge of the device relative to the capacitance of the sensing region. Parallel capacitance is undesirable (from the standpoint of signal-to-noise ratio) but can be tolerated because the pressure-induced capacitance change is designed to be very high, ~ 1 pF mbar^{-1} (see Section 3). One can conceive of more complex designs where the parallel capacitance is much reduced by selective etching or doping in the Si–SiO_2–Si structure. However, for the prototype design, the device structure was kept as simple as possible so that the fabrication procedure was comparatively straightforward.

3. Design considerations

3.1. Pressure sensitivity dependence on structure

Many pressure sensors in the literature (e.g., [6,18,7,19]) and many commercial ones have square diaphragms because this shape is easily made with standard KOH etchant and gives rise to a high stress distribution suitable for piezoresistors. However, for capacitive sensors, a circular diaphragm is better: it is about twice as strong as a square diaphragm, and provided the structure is optimized over a particular pressure range, sensitivity is similar.

Pressure sensitivity as a function of capacitance has been discussed elsewhere as somewhat complicated analytical functions or numerical formulations (e.g., [20]). Here a simple, generalized trigonometric analytical relationship is derived for a circular diaphragm capacitance pressure sensor. Small deflections, $W(r)$, at radius r, on a circular plate of constant thickness under axisymmetric pressure loading are given by [21]

$$\nabla^4 W = \frac{1}{r}\frac{\mathrm{d}}{\mathrm{d}r}\left\{r\frac{\mathrm{d}}{\mathrm{d}r}\left[\frac{1}{r}\frac{\mathrm{d}}{\mathrm{d}r}\left(r\frac{\mathrm{d}W}{\mathrm{d}r}\right)\right]\right\} = \frac{P(r)}{D} \quad (1)$$

where $D = Eh^3/12(1-\nu^2)$ is the flexural rigidity (for which E is Young's modulus, h is the plate thickness, and ν is Poisson's ratio). For a uniform pressure loading P, the deflection $W(r)$, on a circular diaphragm of radius R, is derived from repeatedly integrating Eq. (1) to give

$$W(r) = \frac{P(R^2 - r^2)^2}{64D} \quad (2)$$

The pressure-sensitive capacitance of the area underneath the diaphragm is given by

$$C = 2\pi\epsilon_0 \int_0^R \frac{r\,\mathrm{d}r}{d_0 - W(r)} \quad (3)$$

where d_0 is the distance between the diaphragm and fixed plate at zero pressure difference and ϵ_0 is the permittivity of free space. By combining Eqs. (2) and (3), we get

$$C = 2\pi\epsilon_0 \int_0^R \frac{64Dr\,\mathrm{d}r}{64Dd_0 - PR^4(1-(r/R)^2)^2} \quad (4)$$

If we make the substitution $Z = 1-(r/R)^2$ then

$$C(Z) = C_0 \int_0^1 \frac{\mathrm{d}Z}{1-(P/P_{\max})Z^2} \quad (5)$$

where $C_0 = (\pi R^2\epsilon_0)/d_0$ is the zero-pressure parallel-plate capacitance and

$$P_{\max} = (64Dd_0)/R^4 \quad (6)$$

is the pressure at which the diaphragm touches the underlying substrate. By putting $y = P/P_{\max}$, and evaluating the integral, the capacitance as a function of fractional pressure, y, can be simply expressed as

$$C(y) = C_0\left(\frac{1}{y^{1/2}}\right)\tanh^{-1}(y^{1/2}) + C_p + C_s \quad (0 \le y \le 1) \quad (7)$$

where the additional terms, which have been hitherto ignored, are C_p, the parallel capacitance of the square chip surrounding the circular, pressure-variable sensor capacitance, and C_s, the parallel capacitance between the leads. C_p and C_s act as static offsets. The fractional distance moved by the centre of the diaphragm is also equivalent to y, i.e., $y = W_c/d_0$, where W_c is the centre deflection. For mathematical completeness, in a real sensor, the sealed internal reference pressure, P_{int} will never be exactly zero so that if P_{ext} represents the external applied pressure, we make the correction that

$$y = \frac{P_{\text{ext}} - P_{\text{int}}}{P_{\max}} \quad (8)$$

If $P_{\text{ext}} < P_{\text{int}}$, $y^{1/2}$ becomes imaginary, but if we substitute the identity $-i\tan^{-1} \equiv \tanh^{-1} z$ (where $i = (-1)^{1/2}$) in Eq. (7) then we can evaluate the capacitance in this regime according to

$$C(y) = C_0\left(\frac{1}{(-y)^{1/2}}\right)\tan^{-1}((-y)^{1/2}) + C_p + C_s \quad (y \le 0) \quad (9)$$

One further complication with the devices that were actually fabricated is that some had thin layers residing in the base of the cavity (e.g., SiO_2 resulting from fusion bonding in oxygen). In the general case where there are thin layers of materials a, b, c, ..., with thicknesses $d_a, d_b, d_c, \ldots$, and with relative permittivities, $\epsilon_{ra}, \epsilon_{rb}, \epsilon_{rc}, \ldots$, the capacitance will be

$$C(y) = C_{c0}\left(\frac{K_d}{y}\right)^{1/2}\tanh^{-1}\left(\frac{y}{K_d}\right)^{1/2} + C_p + C_s \quad (0 \le (y/K_d) \le 1) \quad (10)$$

$$C(y) = C_{c0}\left(-\frac{K_d}{y}\right)^{1/2}\tan^{-1}\left(-\frac{y}{K_d}\right)^{1/2} + C_p + C_s \quad ((y/K_d) \le 0) \quad (11)$$

Here, K_d, a 'series dielectric correction', is given by

$$K_d = 1 + \frac{1}{d_0}\left(\frac{d_a}{\epsilon_{ra}} + \frac{d_b}{\epsilon_{rb}} + \ldots\right) = 1 + \Delta \quad (12)$$

where generally $\Delta \le 0.1$, and the parallel-plate capacitance (at $P_{\text{ext}} = P_{\text{int}}$) is now $C_{c0} = C_0/K_d = (\epsilon_0\pi R^2)/(K_d d_0)$.

Eqs. (7)–(12) are useful mathematical summaries of the response of a capacitive pressure sensor in the regime where the diaphragm is not touching the substrate (plotted in Fig. 2). However, according to the basic capacitance response to pressure (Eq. (7)), the capacitance increases without bound when $y \to 1$. In reality, the capacitance reaches some finite value before the diaphragm touches the substrate because of electrostatic effects combined with surface roughness: complex phenomena which have been omitted. Therefore this analytical model only applies for that region of the sensor response at pressures before the diaphragm becomes appreciably close to the underlying substrate. Also, this analysis assumes that the diaphragm is not pre-stressed.

At low pressures (i.e., $0 < y \ll 1$) the first-order linear response to pressure can be found using the expansion $\tanh^{-1}(z) = z + z^3/3 + z^5/5 + \ldots$ in Eq. (7) to give

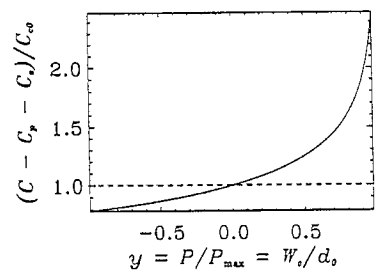

Fig. 2. A dimensionless pressure–capacitance curve. Here the dashed line indicates the capacitance when the diaphragm is parallel to the substrate at zero differential pressure. The curve below this line is applicable only if the diaphragm is bowing outwards due to mounting stress or internal pressure.

$$C \approx C_{c0}\left[1+\frac{1}{3K_d}\left(\frac{P}{P_{max}}\right)\right] \quad (13)$$

Moreover, an exact expression for the sensitivity to pressure (in terms of pF mbar^{-1}, say) at the zero pressure point, $P=0$, is given by

$$\frac{dC}{dP}=\frac{1}{3}\left(\frac{C_0}{P_{max}}\right) \quad (P=0, K_d=1) \quad (14)$$

Since the practical resolution of a pressure sensor depends on the capability of the readout circuitry to discriminate changes in capacitance, it is desirable to make dC/dP as large as possible. Because this is inversely proportional to the touching pressure, P_{max}, it is advantageous to make P_{max} smaller than 1 bar for a sensor designed for the vacuum range to ensure high sensitivity. For the sensors investigated in this paper, P_{max} was made small by using a large-diameter diaphragm (2–3.4 mm) combined with a sub-micron capacitance gap, d_0. For example, if dimensions are selected so that $C_0 \sim 150$ pF and $P_{max} \sim 100$ mbar, then we calculate an output of 0.5 pF mbar^{-1} near zero pressure; consequently, to obtain a resolution of 0.01 mbar we would need to measure changes of 0.005 pF, which is readily achievable. Of course, due to the nonlinear nature of capacitive pressure sensors, the sensitivity will increase with pressure. By differentiating Eq. (7) with respect to applied pressure, we can determine this increase. For the aforementioned sensor, the sensitivity at 10 mbar is calculated to be 0.57 pF mbar^{-1} compared to 0.5 pF mbar^{-1} at zero pressure. As noted in Section 1, for sensors that are individually calibrated, nonlinearity is not a problem provided that it is repeatable.

3.2. Mechanical strength of the transducer

An important design consideration for a large-area thin-diaphragm sensor is the pressure that causes diaphragm breakage. Silicon undergoes no plastic flow (except at temperatures >600°C) and for (100) silicon wafers the fracture stress in the [110] direction is the elastic limit, typically several GPa [22,23]. The maximum stress is exerted along the edge of the circular diaphragm and in the regime where the diaphragm is freely deflecting it can be calculated analytically [24]. However, the construction of the capacitance sensor in this paper incorporated a diaphragm stop. Calculations for such a nonlinear contact problem were done using a finite-element analysis (FEA) software package, ANSYS. In the FEA model, the diaphragm was loaded to greater than 1 bar pressure so that its centre squashed flat against the contact surface. The maximum stress in the diaphragm structure at high overpressures was compared with the fracture stress of silicon. Due to symmetry about a central axis, a simplification was to model the diaphragm by using a 2-D axisymmetric isoparametric solid element. The contact surface was modelled using rigid 2-D contact surface elements that resist penetration. The model also incorporated the simplifying assumption that the edge of the circular diaphragm remained rigidly fixed. This assumption causes an overestimate for the stress at the edge of the deflected diaphragm (by ~10%) because in actuality there is some 'give' in the support structure. However, since the purpose of the FEA was to overdesign the pressure sensor structure to withstand high overpressure, these simplifications posed no concern.

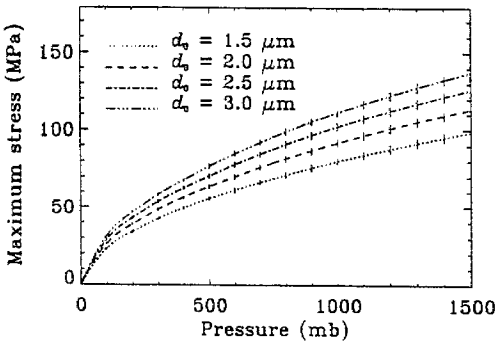

Fig. 3. Maximum diaphragm (radial) stress in sensor structures as the pressure is increased from 0 to 1500 mbar. The diaphragm diameter was 3.4 mm and its thickness was 20 μm. The cavity gap, d_0, was varied as shown.

Various device structures with diaphragm diameter, a, from 1.0 to 4.0 mm, diaphragm thickness, h, from 10 to 30 μm, and sensor cavity depth, d_0, from 0.5 to 3 μm, were evaluated. For each specific sensor structure (i.e., each combination of a, h and d_0), the diaphragm was loaded from 0–1500 mbar in steps of 100 mbar and the maximum stress endured at each 100 mbar pressure step was output. Fig. 3 is an example plot showing the effect of varying the cavity gap, d_0, on the maximum stress in a sensor structure with a silicon diaphragm of 3.4 mm diameter and 20 μm thickness. The maximum stress increases linearly with pressure up the point where the silicon diaphragm touches the opposing substrate and beyond this point the diaphragm stress increases nonlinearly with pressure at a much lower rate because the diaphragm stop provides a reaction force. For the weakest structure in Fig. 3, a maximum diaphragm stress of 1 GPa (assumed close to fracture) is not reached until a pressure of 77 bar is applied. Similar results were obtained within the realm of parameter space investigated. Consequently, thin large-area diaphragm structures (necessary for high sensitivity) with a diaphragm stop are very strong. Thus structural strength posed no concern; indeed, fabricated sensors have proved extremely robust in handling.

3.3. Design rules

There are three parameters to vary in the sensor construction: diaphragm thickness, capacitance cavity depth, and diaphragm(/cavity) diameter. The dimensions for the sensors that were made, although partly arbitrary, were chosen according to the following criteria based on performance expectations and practical limits imposed by process technology. As a rough guide, the sensor had:

- a 'sizeable' diaphragm diameter ($a=2.5$–3.5 mm) for high sensitivity, since the sensitivity is proportional to a^4.
- a relatively thick diaphragm ($h>15$ μm) for robustness

- a small capacitance gap ($d_0 < 1.5$ μm). The upper limit was constrained by the process technology because d_0 was defined by the depth of the SiO_2 SEMIROX dielectric layer and this could only be grown reliably in a reasonable time for thicknesses < 2 μm. A very small gap gives much strength and enlarges the size of the capacitance change one must detect for a given resolution. However, if the gap is too small (< 0.3 μm) dust contamination in the cavity becomes very likely.

For the purpose of validating both the technology and design, sensors were made with a variety of dimensions selected subject to the criteria above. The pressure, P_{max}, at which the diaphragm touches the substrate beneath it, ranged from about 40 mbar to greater than 1 bar in the various structures. For low-pressure sensors, the increase in capacitance (using Eq. (10)) above the offset capacitance was typically around 10 or 20 pF over the range of interest, 0–12 mbar.

4. Sensor fabrication

The micromachining steps in making the transducer started with the local oxidation of silicon (LOCOS) process [25] necessary to produce circular cavities in SEMIROX across a wafer. First, nitride growth (0.16 μm) followed by photolithography and plasma etching produced circular sections of nitride across a wafer surface. A SEMIROX layer was grown around the nitride sections at 1100°C. Plasma etching was then used to remove the nitride film. This left circular holes in the SEMIROX layer. The thickness of this SEMIROX layer was varied in two batches to be 1.2 and 2.1 μm, leading to cavities of depth 0.44 and 0.80 μm, respectively, measured with SEM. Next these patterned wafers were fusion bonded to blank wafers.

The SFB process required a class 10 environment because the cavities were of large area and small depth, so that any dust particles sealed within them would prevent free movement of the silicon diaphragm with pressure. The fusion bond was checked with acoustic microscopy and it was found with trial wafers that SFB under high-vacuum conditions often led to poor bonding. Wafers tended to be bonded at the centre only, and would separate if the upper wafer was later subjected to KOH etching. However, a dry oxygen environment was found to give good bonding: 80–100% of the area across a wafer pair was bonded. Bonding in 1 atm oxygen leads to vacuum cavities because the oxygen gets consumed in the bonding process to form SiO_2 on the interior surfaces of cavities. A low-pressure oxygen environment (0.1–1 mbar) for SFB was also found to be successful. Low-pressure oxygen may be preferred to using 1 atm to reduce the level of gaseous impurities (e.g., N_2) sealed within the cavity. The SFB process consisted of megasonically cleaning wafers, rinsing them in deionized water, spin drying, and then mating the wafers in a jig under low-pressure oxygen. Subsequent heating to 1150°C for 3 h was necessary to form the bond.

Afterwards, the upper silicon wafer in the bonded pair was thinned using a KOH timed etch. In different batches, thicknesses of 30 and 52 μm were produced. Subsequently, aluminium contacts were deposited, followed by dicing. Prior to dicing, some wafers were cleaved at their edges to facilitate SEM measurement of cavity depth, SEMIROX thickness, and diaphragm thickness. These measurements were later used to interpret device behaviour. Some chips taken from the centre of the wafer were also individually cleaved and measured with SEM. Finally, for convenience, the silicon chips were mounted on TO5 transistor heads.

5. Preliminary results

Sensors were tested in a vessel with pressure control from $< 10^{-5}$ mbar up to 1050 mbar and temperature control to ±0.5 K over 150–300 K using a liquid-nitrogen cryostat. A commercial digital meter was used for measuring the capacitance of each transducer at 10 kHz with four coaxial wires per sensor to eliminate lead impedances. Two MKS Baratrons were used for reference pressure measurement over 0–14 mbar (with 0.001 mbar resolution) and 0–1050 mbar (with 0.1 mbar resolution), respectively. Bad sensors were first screened out by checking for basic functionality. Some devices were found to suffer from very small sensitivity to pressure loading and/or high hysteresis. Although sensors were formed from wafers bonded in class 10 conditions, the most likely explanation is internal contamination by dust particles comparable in size to the sub-micron cavities which impeded the diaphragms from deflecting.

5.1. Pressure–capacitance measurements

To check for hysteresis, capacitance was measured at static pressure points from $< 10^{-5}$ mbar to 1000 mbar and then back down in pressure at room temperature, ~20°C, with measured ambient temperature variations < 0.5°C. Fig. 4(a) shows a typical response over 1 bar for a sensor with diaphragm diameter $a = 3.2$ mm, diaphragm thickness $h \sim 30$ μm, and cavity depth $d_0 = 0.44$ μm. The sensor has the characteristic pressure–capacitance curve up to a point of inflection at which the diaphragm touches the opposing substrate. At higher pressures, because of the thin SiO_2 film at the bottom of the cavity from SFB, the capacitance increases linearly at first as contact area increases. Subsequent capacitance increase is highly nonlinear because the diaphragm becomes stressed at its edges and resists further bending. When the pressure is lowered, the diaphragm can 'stick' a little to the bottom of the cavity, which results in hysteresis in this contact regime (i.e., the capacitance is slightly higher on the decreasing pressure curve). However, eventually the diaphragm springs back up into its freely deflecting position. In this low-pressure regime (Fig. 4(b)) where the transducer is designed to be used, readings were repeatable with high sensitivity ~0.75 pF $mbar^{-1}$ at 0 mbar. Fig. 5(a) shows the

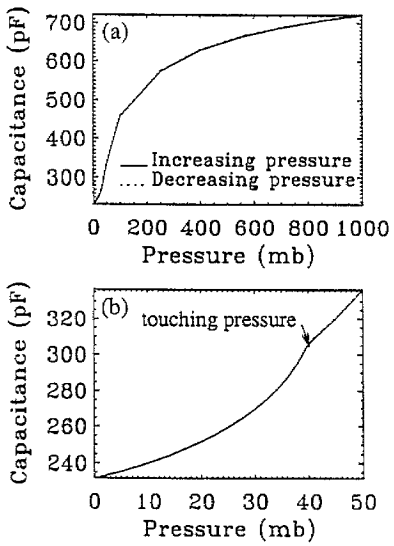

Fig. 4. (a) The capacitance–pressure response for a sensor where the pressure was varied from high vacuum to 1 bar and back. (b) A more detailed plot showing the low-pressure region. The chip is designed to operate over 0–12 mbar.

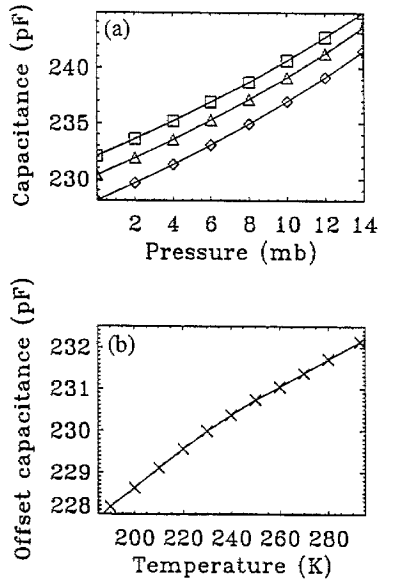

Fig. 5. (a) Measurements illustrating the change in sensitivity with temperature over a range of ~100 K (□ = 293 K, △ = 240 K, ◇ = 190 K). (b) The offset change with temperature of the same sensor (under high vacuum).

same sensor tested under different temperatures of 293, 240, and 190 K over the design range of pressure. The sensitivity changes negligibly with temperature but the offset changes nonlinearly, as plotted in Fig. 5(b), by ~0.04 mbar K^{-1} to first order.

5.2. *Application of analytical theory to experiment*

A notable aspect of Fig. 4(b) is that the measured touching pressure, ~40 mbar, is higher than that calculated from Eq. (6), ~20 mbar, from the dimensions of the sensor diaphragm and cavity measured with SEM. However, this sensor was mounted on a transistor header with fast-set epoxy for convenience. Most likely the stress of mounting caused the centre of the diaphragm to bow outward by a distance comparable to the cavity depth. A multivariate nonlinear least-squares fit (using the Marquardt method [26]) allowed the simple arctanh curve of Eq. (10) to be fitted to the experimental curve of Fig. 4(b) with $P_{max} = 19.7$ mbar, provided an initial diaphragm outward central deflection of 0.58 μm (compared to the diaphragm diameter of 3400 μm) was included. Fig. 6 shows the capacitance–pressure response for a sensor mounted using softer room-temperature-setting glue and a nonlinear least-squares fit to the measurements. This sensor had a diaphragm diameter 2.6 mm, diaphragm thickness 52 ± 3 μm, cavity depth of 0.82 ± 0.02 μm, and a measured touching pressure at ~168 mbar. The arctanh curve was fitted with parameters $C_{c0} = 60.6 \pm 0.7$ pF, $C_p = 151 \pm 1$ pF, and $P_{max} = 170.18 \pm 0.02$ mbar; $\chi^2 = 0.06$. These compare with calculated values of $C_{c0} = 57.3 \pm 1.4$ pF, $C_p = 159 \pm 8$ pF, and $P_{max} \sim 402$ mbar, from sensor dimensions. Clearly, this sensor demonstrates behaviour which is dissimilar to that of the sensor of Fig. 4(b) because the diaphragm touches the opposing substrate at a lower pressure than calculated. Thus the response of these high-sensitivity low-pressure sensors is strongly influenced by the method used to mount them. Nevertheless, behaviour can be characterized by a simple analytical function.

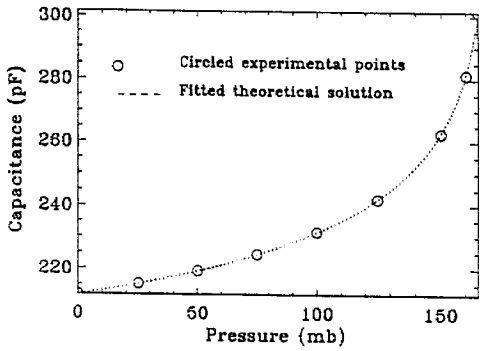

Fig. 6. A nonlinear least-squares fit of Eq. (10) to sensor data (see text).

6. Conclusions

The motivation for this investigation was to examine sensors that may be suitable for highly sensitive measurements of the barometric pressure on Mars (a few millibars). The sensor is also required to be robust. A simple capacitive prototype, consisting of a circular silicon diaphragm that deflects with applied pressure towards a fixed silicon substrate, was investigated. The capacitance gap is a sealed vacuum cavity so that the device senses absolute pressure. Dimensions were selected so that the diaphragm touched the opposing substrate at vacuum pressures down to 40 mbar, leading to high sensitivity at pressures of 0–10 mbar.

The theoretical pressure resolution, capacitance versus pressure response, and mechanical strength were discussed. Finite-element structural analysis shows such sensors to be

particularly resistant to overpressure because diaphragm movement is constrained to sub-micron distances by a diaphragm stop. Typically, sensors are calculated to fracture at a pressure of many tens of bar. The fabrication of the silicon device included silicon fusion bonding effected under oxygen. The oxygen assists in the bonding process and gets consumed to leave vacuum cavities. Bonding under high vacuum was consistently found to be poor, apparently at odds with successful bonding of this nature reported elsewhere [27]. Fusion bonding reduces thermal mismatch in the sensor die and provides for long-term stability of the sealed cavity.

Sensors broadly showed the expected behaviour under test: the capacitance increases with pressure according to a derived arctanh relationship up to a point of inflection where the diaphragm contacts the underlying surface. Large-diaphragm sensors (>3 mm diameter) have a measured sensitivity of typically 0.7–1 pF $mbar^{-1}$ in the range of interest (0–12 mbar) where the diaphragm freely deflects. In the regime of diaphragm–substrate contact (above the range of interest) considerable hysteresis was found because the diaphragm 'sticks' to the surface and draws off more slowly with decreasing pressure. This implies that capacitive sensors that actually use this mechanism, as suggested in Refs. [28–30] for enhanced linearity, are likely to have poor repeatability.

Generally, sensors exhibited behaviour consistent with effects caused by mounting stress, which is particularly influential for such highly sensitive devices. In the preliminary results discussed here, no special attention was given to sensor chip mounting but low-stress mounting is crucial in further development of these devices (or other low-pressure sensors) to reduce temperature dependence and long-term zero drift from gradual stress relaxation. Further work will assess a variety of soft mounting techniques (e.g., with RTV silicone rubber or dielectric gel) and their effects on pressure-sensor response. It is anticipated that offset sensitivity to temperature (~ 0.04 mbar K^{-1} for a device simply mounted with epoxy) could be greatly reduced with careful mounting. Additional work includes monitoring the long-term zero drift of the devices, which is also likely to depend on the mounting technique. Possible interface microelectronics were not discussed in this paper but appropriate capacitance-to-voltage ICs are now available commercially (e.g., CSEM2003D available from Centre Suisse d'Electronique et de Microtechnique or TI28882D from Texas Instruments Japan).

Acknowledgements

This work was completed while the author held a National Research Council–NASA Ames Research Associateship. Sensor fabrication was supported by the UK Science and Engineering Research Council (SERC) while the author was at the University of Oxford. Particular thanks to Jean Humphrey (Southampton University) and Russell Craddock (Druck Ltd.) for sensor fabrication. Thanks to the Rutherford Appleton Laboratory for photomasks. Thanks to Gongui Gin and Professor Harold Gamble at The Queen's University of Belfast for silicon bonding. Thanks also to: Simon Calcutt, Ish Aslam, and Professor Fred Taylor at Oxford; Angela MacManus, Andrew Jury, and Alan Evans at Southampton; and Mike Bertioli and John Greenwood at Druck.

References

[1] R.M. Haberle and D.C. Catling, A micro-meteorological mission for global network science on Mars: rationale and measurement requirements, Planet. Space Sci., 44 (1996) 1361–1383.
[2] S.C. Merrihew, R.M. Haberle and L.G. Lemke, A micro-meteorological mission for global network science on Mars: a conceptual design, Planet. Space Sci., 44 (1996) 1385–1393.
[3] K.E. Petersen, Silicon as a mechanical material, Proc. IEEE, 70 (1982) 420–457.
[4] R.M. Langdon, in R.A. Levy, (ed.), Novel Silicon Based Technologies, Kluwer, London, 1991, pp. 143–172.
[5] S. Middelhoek and S.A. Audet, Silicon Sensors, Academic Press, London, 1989.
[6] C.S. Sander, J.W. Knutti and J.D. Meindl, A monolithic capacitive pressure transducer with pulse-period output, IEEE Trans. Electron Devices, ED-27 (1980) 927–930.
[7] M.J.S. Smith, L. Bowman and J.D. Meindl, Analysis, design and performance of a capacitive pressure sensor IC, IEEE Trans. Biomed. Eng., BME-33 (1986) 163–174.
[8] R. Puers, Capacitive sensors: when and how to use them, Sensors and Actuators A, 37–38 (1993) 93–105.
[9] P. Renaud, CSEM, Capteur de mesure de pression absolue de type capacitif et procede de fabrication d'une pluralite de tels capteurs, French Patent No. 93 01700 (19 May, 1995).
[10] F. Rudolf and H. de Lambilly, Low-cost pressure sensor microsystem, Proc. Microsystems Technologies '94, Berlin, Germany, Oct. 1994, pp. 703–705.
[11] H. Chau and K.D. Wise, Scaling limits in batch-fabricated silicon pressure sensors, IEEE Trans. Electron Devices, ED-34 (1987) 850–858.
[12] S. Suzuki, K. Yamada, M. Nishihara, H. Hachino and S. Minorikawa, Structural analysis of a semiconductor pressure sensor, Proc. 1st Sensor Symp., Japan, June 1981, pp. 131–133.
[13] T. Rogers, Considerations of anodic bonding for capacitive type silicon/glass sensor fabrication, J. Micromech. Microeng., 2 (1992) 164–166.
[14] T. Rogers and J. Kowal, Selection of glass, anodic bonding conditions and material compatibility for silicon–glass capacitive sensors, Sensors and Actuators A, 46–47 (1995) 113–120.
[15] K. Petersen, P. Barth, J. Poydock, J. Brown, J. Mallon and J. Bryzek, Silicon fusion bonding for pressure sensors, Proc. IEEE Solid-State Sensor and Actuator Workshop, Hilton Head Island, SC, USA, 6–9 June, 1988, pp. 144–147.
[16] P.W. Barth, Silicon fusion bonding for the fabrication of sensors, actuators and microstructures, Sensors and Actuators, A21–A23 (1990) 919–926.
[17] S. Bengtsson, Semiconductor wafer bonding: a review of interfacial properties and applications, J. Electronic Materials, 21 (1992) 841–862.
[18] Y.S. Lee and K.D. Wise, A batch-fabricated silicon capacitive pressure transducer with low temperature sensitivity, IEEE Trans. Electron Devices, ED-29 (1982) 42–48.
[19] A. Jornod and F. Rudolf, High-precision capacitive pressure sensors, Sensors and Actuators, 17 (1989) 415–421.
[20] W.H. Ko, M.H. Bao and Y.D. Yong, A high-sensitivity integrated-circuit capacitive pressure transducer, IEEE Trans. Electron Devices, ED-29 (1982) 48–56.

[21] R.T. Fenner, Engineering Elasticity: Application of Numerical and Analytical Techniques, Ellis Horwood, Chichester, 1986.
[22] S. Johansson, F. Ericson and J.-A. Schweitz, Influence of surface coatings on elasticity, residual stresses, and fracture properties of silicon microelements, J. App. Phys., 65 (1989) 122–128.
[23] F. Pourahmadi, D. Gee and K. Petersen, The effect of corner radius of curvature on the mechanical strength of micromachined single-crystal silicon structures, Proc. 6th Int. Conf. Solid-State Sensors and Actuators (Transducers '91), Tokyo, Japan, 11–14 June 1991, pp. 197–200.
[24] S. Timoshenko and S. Woinowsky-Krieger, Theory of Plates and Shells, McGraw-Hill, New York, 1970.
[25] J.A. Appels, E. Kooi, M.M. Paffen, J.J.H. Schatorje and W.H.C.G. Verkuylen, Local oxidation of silicon and its application to semiconductor device technology, Philips Res. Rep., 25 (1970) 118–132.
[26] P.R. Bevington and D.K. Robinson, Data Reduction and Error Analysis for the Physical Sciences, McGraw-Hill, New York, 1992.
[27] R.D. Black, S.D. Arthur, R.S. Gilmore, N. Lewis, E.L. Hall and R.D. Lillquist, Silicon and silicon dioxide thermal bonding for silicon-on-insulator applications, J. Appl. Phys., 63 (1988) 2773–2777.
[28] L. Rosengren, J. Soderkvist and L. Smith, Micromachined sensor structures with linear capacitive response, Sensors and Actuators A, 31 (1992) 201–205.
[29] W.H. Ko, Q. Wang and Y. Wang, Touch mode capacitive pressure sensors for industrial applications, Proc. 7th IEEE Solid-State Sensor and Actuator Workshop, Hilton Head Island, SC, USA, 3–6 June, 1996, pp. 244–248.
[30] W.H. Ko, Q. Wang, Y. Wang and X.X. Huang, Touch mode capacitive pressure sensors for industrial applications, Micro Electro-Mechanical Systems MEMS '97, Nagoya, Japan, 26–30 Jan., 1997, pp. 284–289.

Biography

David Catling received a B.Sc.(Hons.) degree in physics with astrophysics from the University of Birmingham, UK, in 1990, and a D.Phil. in atmospheric physics from the University of Oxford in 1994. He is presently a research associate at NASA Ames Research Center, where his current research interests are in planetary meteorology, the interaction of life-forms with planetary atmospheres, and sensors for planetary science.